Available online at www.sciencedirect.com
SCIENCE DIRECT®
Journal of Solid State Chemistry 178 (2005) 64–71
JOURNAL OF SOLID STATE CHEMISTRY
www.elsevier.com/locate/jssc

Selective reaction and chemical anisotropy in epitaxial bismuth layer-structured ferroelectric thin films

Takayuki Watanabe[a], Hiroshi Funakubo[a,b,*]

[a]*Department of Innovative and Engineered Materials, Interdisciplinary Graduate School of Science and Engineering, Tokyo Institute of Technology, 4259 Nagatsuta-cho, Midori-ku, Yokohama 226-8502, Japan*
[b]*PRESTO, Japan Science and Technology Corporation (JST), 4259 Nagatsuta-cho, Midori-ku, Yokohama 226-8502, Japan*

Received 27 July 2004; received in revised form 11 October 2004; accepted 13 October 2004

Abstract

Bismuth layer-structured ferroelectric thin films consisting of a stacking of pseudoperovskite and bismuth oxide blocks along the *c*-axis were epitaxially grown on single-crystal substrates by metalorganic chemical vapor deposition (MOCVD), and a selective reaction of the bismuth oxide layer with HCl was demonstrated. Epitaxial films with contrasting crystal orientations were used for the acid treatment in order to probe chemical anisotropy. For *a*/*b*-axis-oriented $SrBi_2Ta_2O_9$, $Bi_4Ti_3O_{12}$, and $SrBi_4Ti_4O_{15}$ films with sequential stacking of the two vertical blocks, notable structural selectivity of the reaction was observed only for $SrBi_2Ta_2O_9$. For this film, the pseudoperovskite block remained and the bismuth oxide block was removed, while both blocks of $Bi_4Ti_3O_{12}$ and $SrBi_4Ti_4O_{15}$ dissolved into the acid. In addition to the bismuth, the other cations in the pseudoperovskite blocks, strontium and titanium, also decreased for $Bi_4Ti_3O_{12}$ and $SrBi_4Ti_4O_{15}$. The selective reaction observed for *a*/*b*-axis-oriented $SrBi_2Ta_2O_9$, however, was not observed for *c*-axis-oriented $SrBi_2Ta_2O_9$ films in which the pseudoperovskite and bismuth oxide blocks were stacked horizontally. The results clearly show that $SrBi_2Ta_2O_9$ has sub-nano-order structural selectivity and chemical anisotropy in the unit cell in the reaction with HCl.

Keywords: Intercalation; Proton; Epitaxial film; Layer structure; Bismuth layer-structured ferroelectrics

1. Introduction

The natural superlattice of a bismuth layer-structured ferroelectrics (BLSFs) consists of a stacking of a $(Bi_2O_2)^{2+}$ block and a pseudoperovskite block along the *c*-axis. The chemical formula is widely given as $(Bi_2O_2)^{2+}(A_{m-1}B_mO_{3m+1})^{2-}$, where *A* is a mono-, di-, or trivalent ion, *B* is a tetra-, penta-, or hexavalent ion, and *m* is the number of BO_6 octahedra in the pseudoperovskite layer. More than 50 compounds of this type have been investigated, and a large number are considered ferroelectric. Among them, some BLSF materials such as $SrBi_2Ta_2O_9$ and $(Bi, La)_4Ti_3O_{12}$ are used for ferroelectric random access memory (FeRAM) [1,2].

Tsunoda et al. [3] reported on a HCl treatment for a $SrBi_2Ta_2O_9$ powder. In that work, the $(Bi_2O_2)^{2+}$ layer in the $(Bi_2O_2)^{2+}(SrTa_2O_7)^{2-}$ stacking was preferentially substituted by two protons, giving a new phase of $H_2SrTa_2O_7$. Structural and compositional data of the resultant phase were shown there as well as the selective attack of HCl to the $(Bi_2O_2)^{2+}$ layer. One way to expand the study of the intercalation is to apply the unique approach to BLSF films, especially for epitaxial films with a 3D structural alignment, so as to establish a novel application utilizing the layered structure. If this

*Corresponding author. Department of Innovative and Engineered Materials, Interdisciplinary Graduate School of Science and Engineering, Tokyo Institute of Technology, G1-32, 4259 Nagatsuta, Midori-ku, Yokohama 226-8502, Japan. Fax: +81 45 924 5446.
E-mail address: funakubo@iem.titech.ac.jp (H. Funakubo).

0022-4596/$ - see front matter © 2004 Elsevier Inc. All rights reserved.
doi:10.1016/j.jssc.2004.10.019

technique is applicable to epitaxially grown films, a series of materials with the artificial nano-structure can be developed.

We have reported a novel *a*/*b*-axis-oriented growth of BLSF thin films that involves a long-range lattice matching with a rutile-type oxide layer [4–6]. In the *a*/*b*-axis-oriented growth, the stacking direction of the two blocks is parallel to the substrate surface, and the pseudoperovskite and $(Bi_2O_2)^{2+}$ blocks that naturally ordered at the interface showed a vertically striped cross-section [4]. We confirmed that this approach is valid for $SrBi_2Ta_2O_9$ (SBT, $m = 2$), $Bi_4Ti_3O_{12}$ (BIT, $m = 3$), and $SrBi_4Ti_4O_{15}$ (SBTi, $m = 4$), while they have different unit length along the stacking direction for the pseudoperovskite layer. A vertically striped intergrowth structure with a different in-plane period can be configured changing the m number. Hence, combining the process and the epitaxial thin film growth technique, a self-assembled nano-structure with a potential micro-electronic application can be prepared (Fig. 1).

However, it is not fully clarified yet whether the technique can be applied to any BLSF films, and whether the reaction prefers a specific crystal direction. A question arises as to whether the pseudoperovskite blocks of other BLSFs are still stable with respect to the acid treatment like that of SBT, given that the local crystal structure and the coordination number of the bismuth in the $(Bi_2O_2)^{2+}$ layer are not identical with those of the *A* site. Besides, the reaction appears to continue in SBT powder with random orientation dipped in HCl [3]. Once the stable pseudoperovskite layer spreads over the surface, however, the reaction rate dramatically decreases because of the distinctive selectivity of the reaction. The chemical anisotropy depending on the crystallographic direction reveals the selective reaction at the $(Bi_2O_2)^{2+}$ layer again.

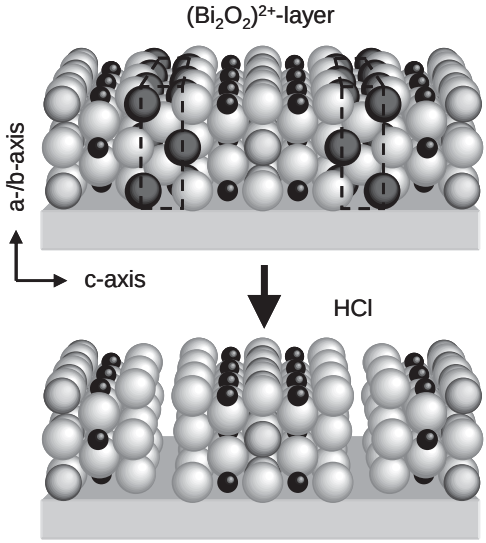

Fig. 1. Schematic crystal structure of an *a*/*b*-axis-oriented BLSF. ($SrBi_2Ta_2O_9$ was drown as a representative material.) Upper and bottom figures show before and after HCl treatment.

In this study, we demonstrate the artificial modification of the epitaxially grown films and the chemical anisotropy in the HCl treatment aiming to supply the basic prospects. Three kinds of high-quality BLSF thin films ($m = 2-4$) were epitaxially grown by metalorganic chemical vapor deposition (MOCVD) to demonstrate the effect of the acid treatment. $SrBi_2Ta_2O_9$ $[(Bi_2O_2)^{2+}(SrTa_2O_7)^{2-}]$, $Bi_4Ti_3O_{12}$ $[(Bi_2O_2)^{2+}(Bi_2Ti_3O_{10})^{2-}]$, and $SrBi_4Ti_4O_{15}$ $[(Bi_2O_2)^{2+}(SrBi_2Ti_4O_{13})^{2-}]$ were used in this investigation. In terms of the constituent cations in the pseudoperovskite layer, the *B* site is tantalum in SBT and titanium in BIT and SBTi. The *A* site is occupied by strontium and/or bismuth. *a*/*b*-axis-oriented epitaxial SBT, BIT, and SBTi films, in which the $(Bi_2O_2)^{2+}$ layer was aligned normal to the substrate surface [5], were used to investigate their structural selectivity in the HCl treatment. In addition, *c*-axis-oriented epitaxial SBT films were prepared in order to characterize the chemical anisotropy by comparing them with the *a*/*b*-axis-oriented films [9].

2. Experimental

$SrBi_2Ta_2O_9$, $Bi_4Ti_3O_{12}$, and $SrBi_4Ti_4O_{15}$ films were deposited at 600–750 °C by MOCVD. Strontium bis-penthaethoxymethoxyethoxy tantalate {$Sr[Ta(OC_2H_5)_5(OC_2H_4OCH_3)]_2$}, tetraisopropoxy titanium [$Ti(O \cdot i\text{-}C_3H_7)_4$], trisdipivaloylmethanato strontium [$Sr(C_{11}H_{19}O_2)_2$], and trimethyl bismuth [$Bi(CH_3)_3$] (TRI Chemical Laboratory, Inc.) were used as sources for the Sr, Ta, Bi, and Ti, and O_2 gas was used as an oxidant. The reactor pressure was 532 Pa. The constituent phases of the film were characterized by X-ray diffraction (XRD, Philips MRD) using Cu*K*α radiation. Single crystals of $(012)Al_2O_3$, $(101)TiO_2$, and $(100)SrTiO_3$ were used for the epitaxial growth process [4–6]. Although BIT and SBTi films grow on $(101)TiO_2$ substrates with the desired crystal orientation, $(012)Al_2O_3$ was used for monitoring the film composition using X-ray fluorescence (XRF) measurement. XRF (Philips PW2404 and SEIKO Instrument SEA2010) measurements were performed to determine the changes in film composition as a result of the HCl treatment. Sol–gel derived samples were used for the film composition measurement as a standard. The error of the composition measurement is below 2–3%. The 100-nm-thick epitaxially grown films, whose structures were $(100)/(010)SBT//(101)TiO_2$, $(100)/(010)BIT//(012)Al_2O_3$, $(100)/(010)SBTi//(012)Al_2O_3$, and $(001)SBT//(100)SrTiO_3$, were dipped in typical 1-M HCl at room temperature for 42 h in maximum. The XRF measurements were repeated for by removing

specimens from the acid. Before the XRF measurements, the samples were dipped in pure water to remove the HCl. They were then put back into the acid for further reaction after the measurements.

3. Results and discussion

3.1. *a*/*b*-axis-oriented epitaxial growth

Figs. 2 and 3 show the results of X-ray structural analysis of the SBTi, BIT, and SBT films as deposited on the single-crystal substrates. As can be seen in Fig. 2, only 200/020 and 400/040 peaks were observed in the $2\theta-\theta$ scans, indicating that the films were grown with an *a*/*b*-axis orientation. Their subsequent epitaxial growth was confirmed by X-ray pole figure measurements. Fig. 3 shows the X-ray pole figures for 119 SBTi, 117 BIT, and 113 SBT. The set of four point peaks in each figure reveals the epitaxial growth with two-fold in-plane symmetry:

(100)(010)[001]$SrBi_4Ti_4O_{15}$, (100)(010)[001]$Bi_4Ti_3O_{12}$//(012)[100]Al_2O_3, and (100)(010)[001]$SrBi_2Ta_2O_9$//(101)[010]TiO_2.

3.2. HCl treatment

The same films whose characteristics are shown in Figs. 2 and 3 were dipped into 1-M HCl. Fig. 4 shows the relation between the film composition and reaction time for each film. In the case of SBTi and BIT, shown in Figs. 4(a) and (b), respectively, each constituent element decreased while keeping the molar ratio of Bi to Ti constant except for an abrupt decrease at the initial stage. These results suggest that for the SBTi and BIT films, not only the $(Bi_2O_2)^{2+}$ layer but also the pseudoperovskite block reacted with the HCl, and that the constituent cations dissolved into the acid. The correlation of the reaction rate suggests that a compound of Bi and Ti dissolved into the HCl.

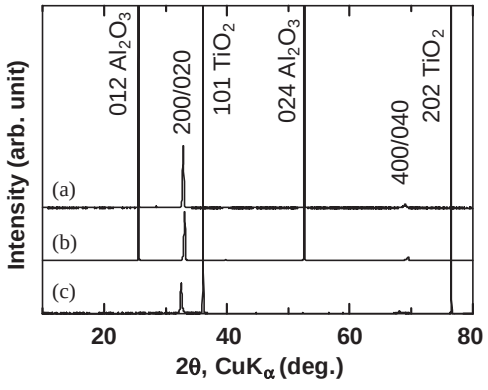

Fig. 2. X-ray diffraction patterns of: (a) $SrBi_4Ti_4O_{15}$/(012)Al_2O_3, (b) $Bi_4Ti_3O_{12}$/(012)Al_2O_3, and (c) $SrBi_2Ta_2O_9$/(101)TiO_2.

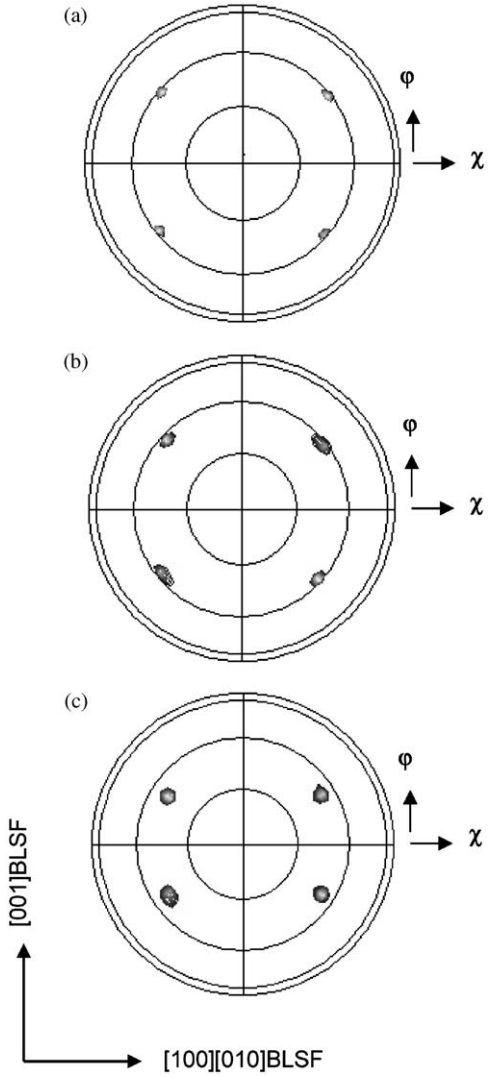

Fig. 3. X-ray pole figure plots of: (a) $SrBi_4Ti_4O_{15}$//(012)Al_2O_3, (b) $Bi_4Ti_3O_{12}$//(012)Al_2O_3, and (c) $SrBi_2Ta_2O_9$//(101)TiO_2. The fixed 2θ angles correspond to (a) 119 $SrBi_4Ti_4O_{15}$, (b) 117 $Bi_4Ti_3O_{12}$, and (c) 113 $SrBi_2Ta_2O_9$.

For the SBT film, the amount of Bi in the $(Bi_2O_2)^{2+}$-layer decreased remarkably as the dipping time increased, while the Sr and Ta, contained in the pseudoperovskite block, remained in the film, as shown in Fig. 4(c). The reduction rate of each element is given by the slope of the natural logarithm of the XRF intensity normalized by the initial value as a function of the dipping time. The degree of structural selectivity of the *a*/*b*-axis-oriented SBT film can be indicated by the ratio of the reduction rate of the Bi to Ta, 8:1. The relative reduction rates for Sr and Ta or Ti are listed in Table 1 and again demonstrate the stability of the $(SrTa_2O_7)^{2-}$ pseudoperovskite block of SBT with respect to the 1-M HCl. The relative reduction rate was given normalizing each reduction rate by that of SBT. According to the literature [3], the resultant SBT

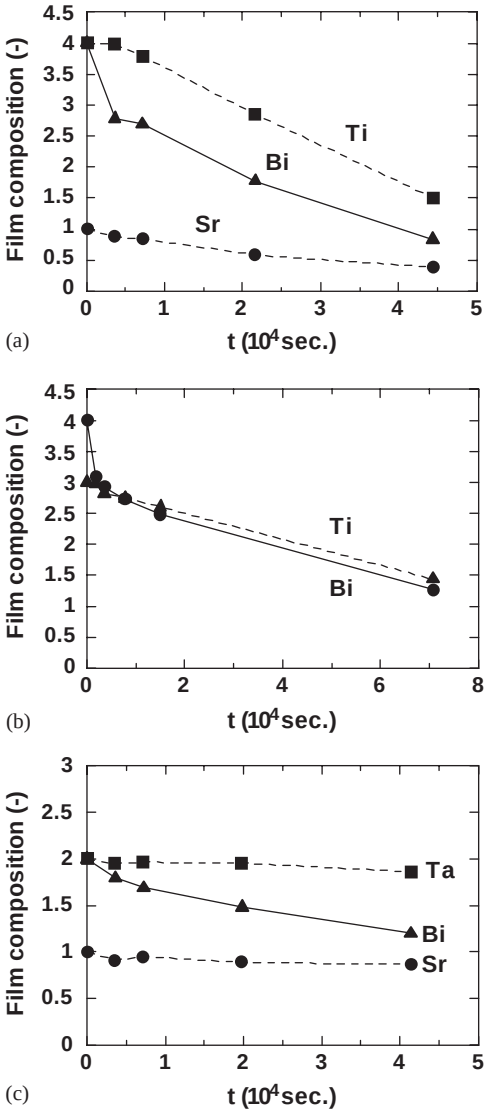

Fig. 4. Time dependence of the metal element composition on the dipping time in 1-M HCl, for starting film compositions of: (a) $SrBi_4Ti_4O_{15}$, (b) $Bi_4Ti_3O_{12}$, and (c) $SrBi_2Ta_2O_9$.

Table 1
Reduction rates of the elements in the pseudoperovskite layer normalized by those of $SrBi_2Ta_2O_9$

Ions	$SrBi_2T_2O_9$	$Bi_4Ti_3O_{12}$	$SrBi_4Ti_4O_{15}$
Sr	1	—	9
Ta/Ti	1(Ta)	6 (Ti)	12 (Ti)

film that lost Bi after the HCl treatment can be understood as a $H_2SrTa_2O_7$ phase; i.e., the $(Bi_2O_2)^{2+}$ layer was removed and two protons were intercalated into that position to compensate for the charge neutrality.

In this study, the selective reaction was observed for SBT ($m = 2$), but not for the BLSF titanate, BIT ($m = 3$) and SBTi ($m = 4$). For the present, reported selective reactions are limited to BLSF tungstate, tantalate, and niobate, i.e., Bi_2WO_6 ($m = 1$), $Bi_2W_2O_9$ with A site vacancies ($m = 2$), $SrBi_2Ta_2O_9$ ($m = 2$), $Bi_2CaNaNb_3O_{12}$ ($m = 3$), and $Bi_2Sr_2Nb_2MnO_{12}$ ($m = 3$) [7–11]. Therefore, the chemical formula of the perovskite-like slab, especially perovskite B site cation, seems to be responsible for the selective reaction rather than the m number. Although the actual bond strengths in the crystal states are not available, we investigated bond enthalpies of diatomic molecules of the cation and an oxygen ion as a parameter of the stability against the acid treatment. The bond enthalpies of WO, NbO, TaO, and TiO diatomic molecules are 672 ± 41.8, 771.5 ± 25.1, 799.1 ± 12.6, and 672.4 ± 9.2 kJ/mol, respectively [12]. The bond enthalpy of TiO is lower than those of NbO and TaO, but comparable to that of WO. On the other hand, those of the perovskite A site are quite lower than those of perovskite B site cations, 425.5 ± 16.7, 402.1 ± 16.7, 256.1 ± 16.7, and 337.2 ± 12.6 kJ/mol for SrO, CaO, NaO, and BiO, respectively [12]. This tendency suggests that the A site cations are responsible for the stability of the perovskite-like slabs rather than the B site cations. The Bi_2WO_6 and $Bi_2W_2O_9$ have no cation in the A site, while the WO bond has the high bond enthalpy as mentioned above. The successful materials for the selective reaction commonly contain no Bi in the perovskite-like slabs. Although the NaO bond is still weaker than that of BiO, we consider that the BiO with low bond enthalpy in the perovskite-like slab affected the leaching of the neighbor Ti from the perovskite-like slabs of the BIT and SBTi films.

3.3. Structural changes resulting from the HCl treatment

Fig. 5 shows enlarged XRD patterns around the 200/020 diffraction measured before and after the HCl treatment. Figs. 5(a) and (b) show a drastic decrease in the 200/020 intensity as a result of the HCl treatment for the SBTi and BIT films, respectively. On the other hand, as shown in Fig. 5(c), a new diffraction peak at a slightly lower angle was found for the HCl-treated SBT film, of which a small amount remained. Tsunoda et al. reported that the resultant artificial phase of $H_2SrTa_2O_7$ is a tetragonal crystal with lattice parameters of $a = 0.391 \pm 0.004$ nm and $c = 0.98 \pm 0.01$ nm (Hereafter, we refer to this phase as HST.) [3]. The diagonal of the a–b plane of HST, [110]HST, corresponds to the original [100]/[010]SBT. The crystal orientation of the HST film transformed from the a/b-axis-oriented SBT film was expected to be (110) keeping the basic structure of the SBT. Fig. 5(c) indicates that the lattice distance of the (110)HST was larger than that of the (200)/(020)SBT. To check the validity of our expectation, we subsequently carried out a detailed structural analysis.

Fig. 6 shows X-ray pole figures measured before and after the HCl treatment. For these measurements, the 2θ

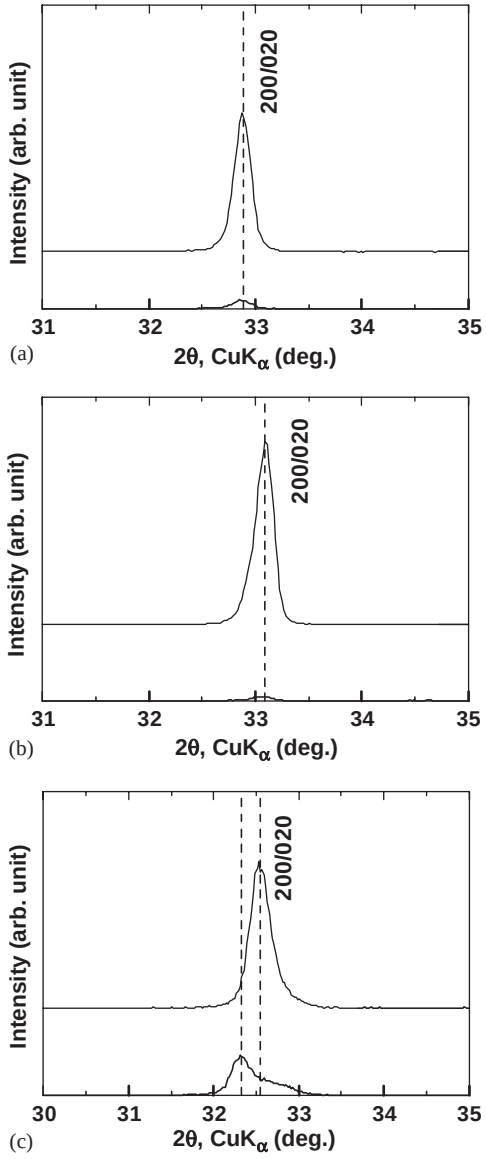

Fig. 5. Expanded X-ray diffraction patterns of: (a) $SrBi_4Ti_4O_{15}$, (b) $Bi_4Ti_3O_{12}$, and (c) $SrBi_2Ta_2O_9$ before (upper) and after (lower) the HCl treatment.

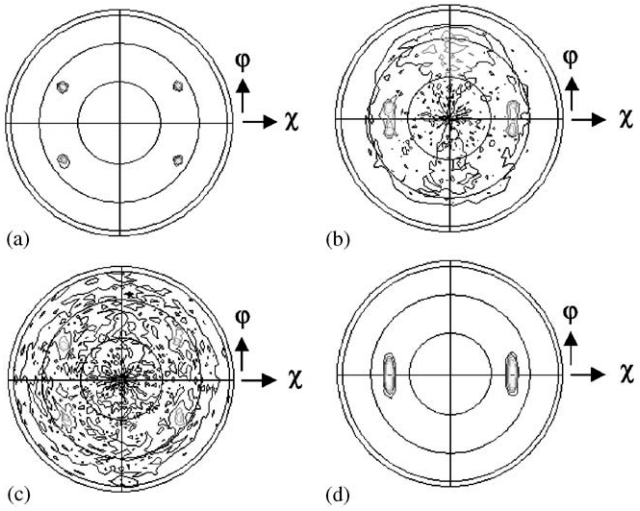

Fig. 6. X-ray pole figure plots of the $SrBi_2Ta_2O_9$ film (a, b) before and (c, d) after the HCl treatment. The fixed 2θ angles were (a, c) 25.1° and (b, d) 22.7°, which correspond to 113 $SrBi_2Ta_2O_9$ and 100 HCl-$SrBi_2Ta_2O_9$.

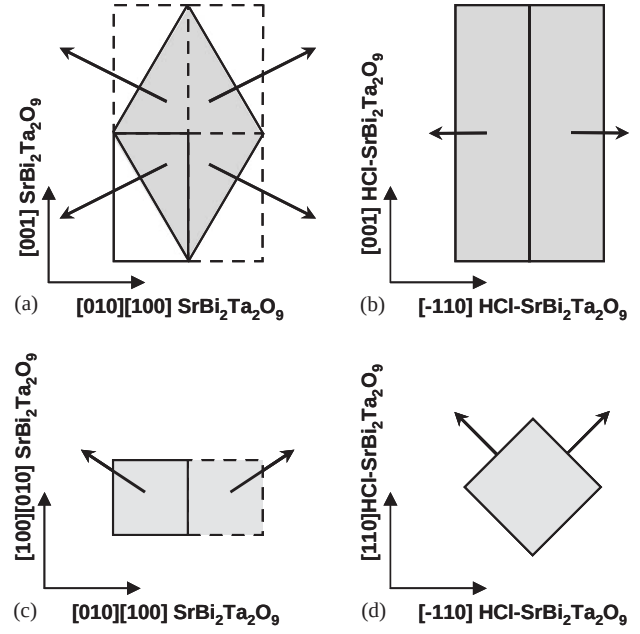

Fig. 7. Schematics of (a, c) the 113 $SrBi_2Ta_2O_9$ plane and (b, d) the 100 HCl-$SrBi_2Ta_2O_9$ plane corresponding to the pole figure plots shown in Figs. 5(a) and 5(d), respectively. The top and bottom figures are plane views and cross-sections, respectively.

angle was fixed to 113 SBT (25.13°) and 100 HST (22.72°) according to calculations using reported lattice parameters [3,13]. Fig. 6(a) corresponds to the *a*/*b*-axis-oriented epitaxial growth of the SBT film and is the same as the pole figure shown in Fig. 3(c). In Fig. 6(b), four weak poles comparable to the background level are observed, although the measurement was made before the HCl treatment. These poles are considered tails of 111 SBT, because the 2θ angle for 111 SBT (22.99°) is close to that for 100 HST (22.72°). The positions of the four weak 111 SBT poles are valid for the *a*/*b*-axis-oriented SBT film.

After the HCl treatment, the four strong poles shown in Fig. 6(a) significantly weakened, as seen in Fig. 6(c). This is in marked contrast to the dramatic change seen in Fig. 6(d), where two strong poles appear after the treatment. These results strongly suggest that the epitaxial *a*/*b*-axis-oriented SBT crystal with two-fold in-plane symmetry changed into an epitaxial (110)HST crystal while maintaining the original basic structure.

Fig. 7 shows schematics corresponding to the pole figure measurements shown in Figs. 6(a) and (d). The

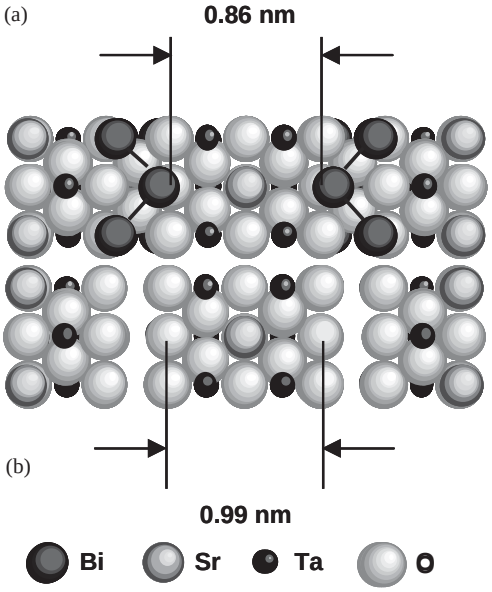

Fig. 8. Schematics of the $SrBi_2Ta_2O_9$ structure (a) before and (b) after the HCl treatment.

arrows drawn in Fig. 7 indicate the diffraction from (113)SBT for Figs. 7(a) and (c) and from (100)HST for Figs. 7(b) and (d). Based on these results, we considered the length of the double octahedron along the *c*-axis. Based on neutron diffraction data [13], the length is 0.86 nm for SBT. From the lattice spacings of (300)HST and (202)HST, as estimated by asymmetric X-ray diffraction, the lattice parameters of the (110)HST film were calculated as $a = 0.3913$ nm and $c = 0.9917$ nm. These values are almost identical to the reported values for powder HST [3]. After the HCl treatment, the length of the double octahedron along the *c*-axis increased to 0.99 nm due to the substitution of the $(Bi_2O_2)^{2+}$ layer by the smaller protons, as shown in Fig. 8.

Here, an interest whether the resultant tetragonal phase has polar class or not arises. It would be possible to probe the ferroelectricity along the surface normal of the (110)HST film fabricating a capacitor structure with a proper bottom and top electrode. The *a*/*b*-axis-oriented films can be grown on several conductive materials [5], e.g., (101)RuO_2 and IrO_2 films grown on the present (101)TiO_2 and (012)Al_2O_3 single crystals substrates. Scanning nonlinear dielectric microscopy is another approach [14]. However, we speculate that the material transformed from polar to non-polar class after the HCl treatment from a crystallographic point of view. The origin of the major spontaneous polarization of BLSFs is the asymmetric crystal structure along the *a*-axis including the rotation and tilting of the perovskite-like slab [13,15]. BLSFs have orthorhombic or more lower crystal symmetry at their ferroelectric state, and transform to a non-ferroelectric tetragonal structure at a ferroelectric/non-ferroelectric phase transition temperature. Consequently, it is difficult to expect a spontaneous polarization for the tetragonal HST phase at least along the *a*–*b*-plane. In this study, we investigated the applicability of the HCl treatment to the three kinds of BLSF thin films directly grown on the single crystal substrates for our first step. Although more detailed structural analysis or direct measurement of the ferroelectricity is still necessary for making it clear, these results will open the door to novel applications utilizing the self-assembled structural features of the HCl-treated BLSFs. For instance, a nano-resistor using the (110)HST epitaxial film can be suggested as a future application. In the nano-resistor, the intercalated proton in the *a*–*b* plane would have a wide range of mobility depending on an external field applied along the rectangular *c*-axis. It may work like a field effect transistor. Changing the applied voltage along the *c*-axis or the value of the stoichiometric parameter *m* would alter the macroscopic conductivity along the *a*–*b* plane.

3.4. Anisotropic reaction rate

In the previous section, the stability of the pseudoperovskite block of SBT with respect to the 1-M HCl was demonstrated by using the *a*/*b*-axis-oriented SBT film. Here, we expected that the stable pseudoperovskite layer would spread over the surface and make the reduction rate remarkably slow. Further investigation of the chemical anisotropy depending on the crystallographic direction could confirm the selective reaction for the $(Bi_2O_2)^{2+}$ layer. Therefore, we deposited a *c*-axis-oriented epitaxial SBT film on a (100)$SrTiO_3$ single-crystal substrate and treated it in the same manner as the *a*/*b*-axis-oriented films [16].

Fig. 9 shows the time-dependent XRF intensities for Ta and Bi for the *a*/*b*-axis-oriented and *c*-axis-oriented SBT films. Because the $SrTiO_3$ single-crystal substrate used for the *c*-axis-oriented film contained Sr, no decrease in Sr from the *c*-axis-oriented SBT film could be observed by the XRF measurement. For Ta, no difference was observed between the two orientations. The Bi in the *c*-axis-oriented SBT film, however, was quite stable as comparing to that in the *a*/*b*-axis-oriented film. In contrast to the *a*/*b*-axis-oriented SBT film shown in Fig. 5(c), the *c*-axis-oriented SBT film demonstrated no obvious change in its XRD measurement after the treatment with 1-M HCl, as shown in Fig. 10. These results indicate that the pseudoperovskite block acted as a capping layer. Table 2 summarizes the crystal orientation dependencies of the reduction rates of Bi and Ta for the SBT films. For the *a*/*b*-axis-oriented SBT film, the Bi decreased four times faster than for the *c*-axis-oriented SBT film. This comparison using two different epitaxial films with contrasting crystal orientations clearly indicated the selective reaction with the

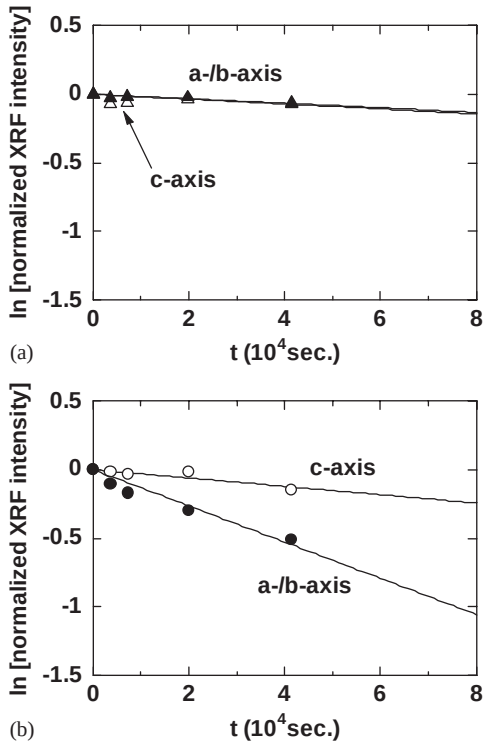

Fig. 9. Normalized X-ray fluorescence intensities of: (a) Ta$K\alpha$ and (b) Bi$M\alpha$ as a function of the HCl treatment time.

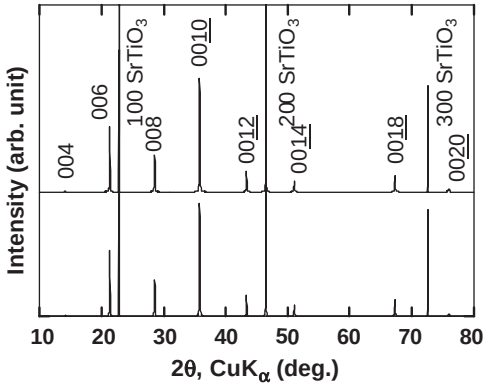

Fig. 10. XRD patterns for the epitaxial *c*-axis-oriented $SrBi_2Ta_2O_9$ film before (bottom) and after (upper) the 1-M HCl treatment.

Table 2
Orientation dependence of the reduction rates of Bi and Ta in the $SrBi_2Ta_2O_9$ films

Ions	*a*-/*b*-axis $SrBi_2Ta_2O_9$	*c*-axis $SrBi_2Ta_2O_9$
Bi	4	1
Ta	1	1

$(Bi_2O_2)^{2+}$ block and the chemical anisotropy in the reaction. These results reveal the possibility of novel applications utilizing the distinctive structural features of bismuth layer-structured ferroelectrics (BLSFs), because there is a variety of BLSFs with different constituent elements and stacking sequence of the two blocks. It is interesting to note that there have been some reports on intergrowth of BLSFs with different values of *m* [17].

4. Conclusions

a/*b*-axis-oriented epitaxial SBT, BIT, and SBTi thin films grown by MOCVD were treated with 1-M HCl. For the SBT film, the acid treatment removed the $(Bi_2O_2)^{2+}$ blocks but left the pseudoperovskite blocks. The *a*/*b*-axis-oriented SBT film was transformed into a tetragonal (110)$H_2SrTa_2O_7$ epitaxial film by the acid treatment maintaining the basic structure of the parent SBT phase. The selective attack of HCl to the $(Bi_2O_2)^{2+}$ is still effective to build up a self-assembled structure using a thin film. On the other hand, the BIT and SBTi films showed no such structural selectivity in the reaction with HCl, i.e., the amounts of all constituent cations of both blocks rapidly decreased. The selective reaction between the $(Bi_2O_2)^{2+}$ block and HCl was not confirmed for the BLSFs that contains bismuth in the pseudoperovskite layer as well as the $(Bi_2O_2)^{2+}$ layer.

Subsequently, we performed the same experiment with a *c*-axis-oriented epitaxial SBT film in order to probe the chemical anisotropy. The preferential decrease of Bi was not observed for this film. The pseudoperovskite blocks, with their superior stability with respect to the HCl treatment, covered the film surface and prevented the decrease in Bi. Consequently, the reaction with HCl preferentially proceeds along the $a-b$ plane. The stability of the pseudoperovskite block against the HCl is significantly responsible for the reaction rate.

Acknowledgments

One of the authors (T.W.) is grateful for receiving research fellowships from the Japan Society for the Promotion of Science for Young Scientists. We also thank Prof. Kinomura, Prof. Kumada, and Dr. Takei of Yamanashi University for their fruitful discussions with us.

References

[1] C.A. Paz de Araujo, J.C. Cuchiaro, L.D. McMillan, M.C. Scott, J.F. Scott, Nature 374 (1995) 627.
[2] B.H. Park, B.S. Kang, S.D. Bu, T.W. Noh, L. Lee, W. Joe, Nature 401 (1999) 682.
[3] Y. Tsunoda, M. Shirata, W. Sugimoto, Z. Liu, O. Terasaki, K. Kuroda, Y. Sugahara, Inorg. Chem. 40 (2001) 5768.
[4] T. Watanabe, H. Funakubo, K. Saito, T. Suzuki, M. Fujimoto, M. Osada, Y. Noguchi, M. Miyayama, Appl. Phys. Lett. 81 (2002) 1660.

[5] T. Watanabe, K. Saito, M. Osada, T. Suzuki, M. Fujimoto, M. Yoshimoto, A. Sasaki, J. Lie, M. Kakihana, H. Funakubo, Proc. Mater. Res. Soc. Symp. 748 (2003) U241.
[6] T. Watanabe, T. Sakai, H. Funakubo, K. Saito, M. Osada, M. Yoshimoto, A. Sasaki, J. Liu, M. Kakihana, Jpn. J. Appl. Phys. 41 (2002) L1478.
[7] R.E. Schaak, T.E. Mallouk, Chem. Mater. 14 (2002) 1455.
[8] R.E. Schaak, T.E. Mallouk, Chem. Commun., 2002, p. 706.
[9] Y. Tsunoda, W. Sugimoto, Y. Sugahara, Chem. Mater. 15 (2003) 632.
[10] M. Kudo, S. Tsuzuki, K. Katsumata, A. Yasumori, Y. Sugahara, Chem. Phys. Lett. 393 (2004) 12.
[11] M. Kudo, H. Ohkawa, W. Sugimoto, N. Kumada, Z. Liu, O. Terasaki, Y. Sugahara, Inorg. Chem. 42 (2003) 4479.
[12] J.A. Kerr, in: D.R. Lide (Ed.), CRC Handbook of Chemistry and Physics, 76th ed, CRC Press, Boca Raton, FL, 1995.
[13] Y. Shimakawa, Y. Kubo, Y. Nakagawa, T. Kamiyama, H. Asano, F. Izumi, Appl. Phys. Lett. 74 (1999) 1904.
[14] H. Odagawa, Y. Cho, Appl. Phys. Lett. 80 (2002) 2159.
[15] Y. Noguchi, M. Miyayama, T. Kudo, Phys. Rev. B 63 (2001) 214102.
[16] K. Ishikawa, H. Funakubo, Appl. Phys. Lett. 75 (1999) 1970.
[17] Y. Noguchi, M. Miyayama, T. Kudo, Appl. Phys. Lett. 77 (2000) 3639.